



**University of Dundee**

## **A Defective Pentose Phosphate Pathway Reduces Inflammatory Macrophage Responses during Hypercholesterolemia**

Baardman, Jeroen; Verberk, Sanne G S; Prange, Koen H M; van Weeghel, Michel; van der Velden, Saskia; Ryan, Dylan G; Wüst, Rob C I; Neele, Annette E; Speijer, Dave; Denis, Simone W; Witte, Maarten E; Houtkooper, Riekelt H; O'Neill, Luke A; Knatko, Elena V; Dinkova-Kostova, Albena T; Lutgens, Esther; de Winther, Menno P J; Van den Bossche, Jan

*Published in:*  
Cell Reports

*DOI:*  
[10.1016/j.celrep.2018.10.092](https://doi.org/10.1016/j.celrep.2018.10.092)

*Publication date:*  
2018

*Document Version*  
Publisher's PDF, also known as Version of record

[Link to publication in Discovery Research Portal](#)

### *Citation for published version (APA):*

Baardman, J., Verberk, S. G. S., Prange, K. H. M., van Weeghel, M., van der Velden, S., Ryan, D. G., ... Van den Bossche, J. (2018). A Defective Pentose Phosphate Pathway Reduces Inflammatory Macrophage Responses during Hypercholesterolemia. *Cell Reports*, 25(8), 2044-2052.e5. <https://doi.org/10.1016/j.celrep.2018.10.092>

### **General rights**

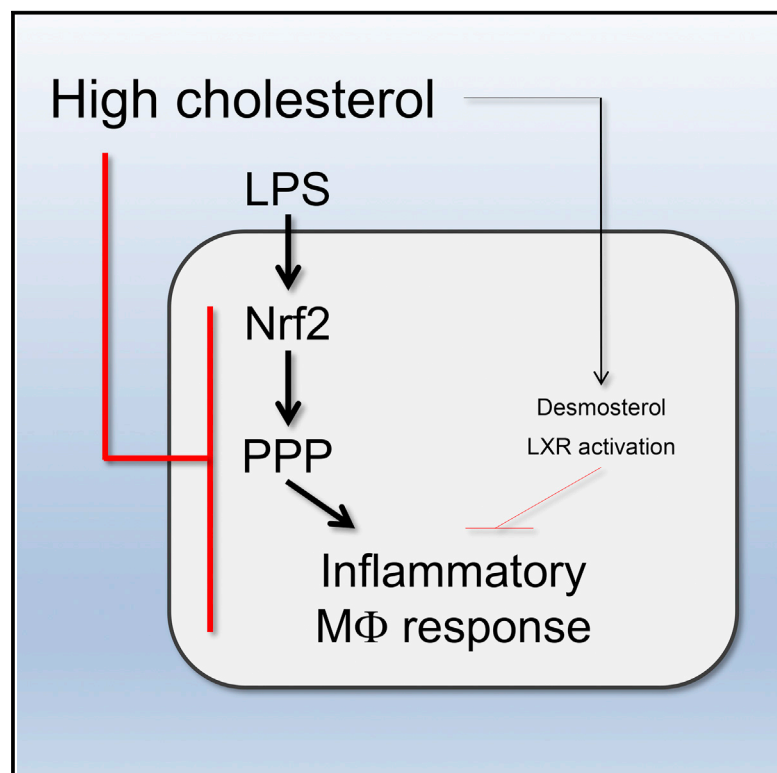
Copyright and moral rights for the publications made accessible in Discovery Research Portal are retained by the authors and/or other copyright owners and it is a condition of accessing publications that users recognise and abide by the legal requirements associated with these rights.

- Users may download and print one copy of any publication from Discovery Research Portal for the purpose of private study or research.
- You may not further distribute the material or use it for any profit-making activity or commercial gain.
- You may freely distribute the URL identifying the publication in the public portal.

# Cell Reports

## A Defective Pentose Phosphate Pathway Reduces Inflammatory Macrophage Responses during Hypercholesterolemia

### Graphical Abstract



### Authors

Jeroen Baardman, Sanne G.S. Verberk, Koen H.M. Prange, ..., Esther Lutgens, Menno P.J. de Winther, Jan Van den Bossche

### Correspondence

j.vandenbossche@vumc.nl

### In Brief

The link between systemic and cellular metabolism is a neglected aspect in immunometabolism. Baardman et al. show that hypercholesterolemia alters macrophage metabolism and phenotype. The suppressed pentose phosphate pathway (PPP) in those “foam cell” macrophages attenuates inflammatory responses, signifying that systemic and cellular metabolism together regulate macrophage function.

### Highlights

- Systemic metabolism affects immune cell metabolism
- Hypercholesterolemia suppresses the PPP and Nrf2 pathway in macrophages
- PPP inhibition and hypercholesterolemia deactivate inflammatory macrophage responses
- The Nrf2 pathway regulates the PPP in an LXR-independent manner



# A Defective Pentose Phosphate Pathway Reduces Inflammatory Macrophage Responses during Hypercholesterolemia

Jeroen Baardman,<sup>1</sup> Sanne G.S. Verberk,<sup>2,9</sup> Koen H.M. Prange,<sup>1,9</sup> Michel van Weeghel,<sup>3</sup> Saskia van der Velden,<sup>1</sup> Dylan G. Ryan,<sup>4</sup> Rob C.I. Wüst,<sup>3,5</sup> Annette E. Neele,<sup>1</sup> Dave Speijer,<sup>1</sup> Simone W. Denis,<sup>3</sup> Maarten E. Witte,<sup>2</sup> Riekelt H. Houtkooper,<sup>3</sup> Luke A. O'Neill,<sup>4</sup> Elena V. Knatko,<sup>6</sup> Albena T. Dinkova-Kostova,<sup>6,7</sup> Esther Lutgens,<sup>1,8</sup> Menno P.J. de Winther,<sup>1,8,9</sup> and Jan Van den Bossche<sup>1,2,9,10,\*</sup>

<sup>1</sup>Amsterdam UMC, University of Amsterdam, Department of Medical Biochemistry, Experimental Vascular Biology, Amsterdam Cardiovascular Sciences, Meibergdreef 9, 1105 AZ Amsterdam, the Netherlands

<sup>2</sup>Amsterdam UMC, Vrije Universiteit Amsterdam, Department of Molecular Cell Biology and Immunology, Amsterdam Cardiovascular Sciences, Cancer Center Amsterdam, De Boelelaan 1117, 1081 HZ Amsterdam, the Netherlands

<sup>3</sup>Amsterdam UMC, University of Amsterdam, Laboratory Genetic Metabolic Diseases, Amsterdam Cardiovascular Sciences, Meibergdreef 9, 1105 AZ Amsterdam, the Netherlands

<sup>4</sup>School of Biochemistry and Immunology, Trinity Biomedical Sciences Institute, Trinity College Dublin, Dublin 2, Ireland

<sup>5</sup>Amsterdam UMC, University of Amsterdam, Department of Biomedical Engineering and Physics, Amsterdam Cardiovascular Sciences, Meibergdreef 9, 1105 AZ Amsterdam, the Netherlands

<sup>6</sup>Jacqui Wood Cancer Centre, Division of Cellular Medicine, School of Medicine, University of Dundee, Dundee DD1 9SY, UK

<sup>7</sup>Department of Pharmacology and Molecular Sciences, Johns Hopkins University School of Medicine, Baltimore, MD 21205, USA

<sup>8</sup>Institute for Cardiovascular Prevention (IPEK), Ludwig Maximilians University, Pettenkoferstrasse 9, 80336 Munich, Germany

<sup>9</sup>These authors contributed equally

<sup>10</sup>Lead Contact

\*Correspondence: [j.vandenbossche@vumc.nl](mailto:j.vandenbossche@vumc.nl)  
<https://doi.org/10.1016/j.celrep.2018.10.092>

## SUMMARY

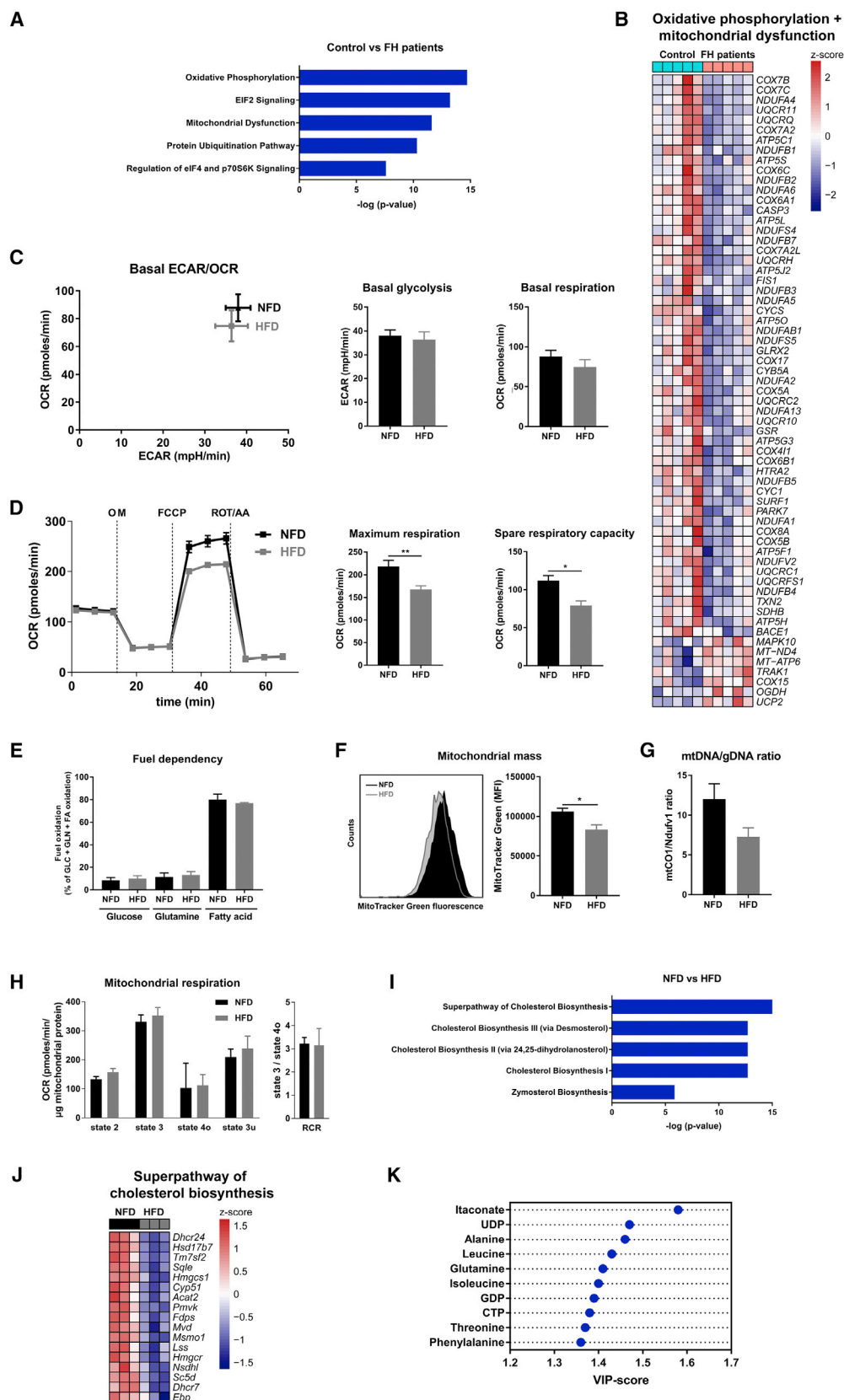
Metabolic reprogramming has emerged as a crucial regulator of immune cell activation, but how systemic metabolism influences immune cell metabolism and function remains to be investigated. To investigate the effect of dyslipidemia on immune cell metabolism, we performed in-depth transcriptional, metabolic, and functional characterization of macrophages isolated from hypercholesterolemic mice. Systemic metabolic changes in such mice alter cellular macrophage metabolism and attenuate inflammatory macrophage responses. In addition to diminished maximal mitochondrial respiration, hypercholesterolemia reduces the LPS-mediated induction of the pentose phosphate pathway (PPP) and the Nrf2-mediated oxidative stress response. Our observation that suppression of the PPP diminishes LPS-induced cytokine secretion supports the notion that this pathway contributes to inflammatory macrophage responses. Overall, this study reveals that systemic and cellular metabolism are strongly interconnected, together dictating macrophage phenotype and function.

## INTRODUCTION

In recent years, metabolic reprogramming arose as a crucial controller of macrophage activation (Van den Bossche et al.,

2016, 2017). For instance, in response to pro-inflammatory stimuli such as the Toll-like receptor 4 (TLR4) ligand lipopolysaccharide (LPS), macrophages show increased glycolysis, as demonstrated by an enhanced extracellular acidification rate (ECAR) (Van den Bossche et al., 2016). Moreover, LPS reconfigures the tricarboxylic acid (TCA) cycle in macrophages and induces itaconate and succinate accumulation (Jha et al., 2015; Tannahill et al., 2013). Itaconate is a key controller of inflammatory macrophage responses through its regulatory effect on succinate dehydrogenase and its activation of the anti-oxidant transcription factor Nrf2 (Lampropoulou et al., 2016; Michelucci et al., 2013; Mills et al., 2018). Succinate promotes inflammation by inducing interleukin 1 $\beta$  (IL-1 $\beta$ ) expression (Mills et al., 2016; Tannahill et al., 2013) and can activate immune cells in the local environment upon secretion (Littlewood-Evans et al., 2016). Furthermore, the activity of the pentose phosphate pathway (PPP) is enhanced in LPS-stimulated macrophages, supplying precursors for nucleotide synthesis and nicotinamide adenine dinucleotide phosphate (NADPH), which is used for reactive oxygen species (ROS) production by NADPH oxidase, fatty acid synthesis, and anti-oxidant cellular defense (Nagy and Haschemi, 2015; Wu et al., 2008). So far, most knowledge regarding macrophage immunometabolism was obtained with *in vitro*-cultured bone marrow-derived macrophages and largely ignored the possible systemic and micro-environmental effects on macrophage metabolism and function *in vivo* (Norata et al., 2015). Exploring this neglected aspect of immunometabolism might identify therapeutic strategies to dampen chronic inflammatory diseases such as atherosclerosis, in which lipid-laden macrophage “foam cells” are crucial during all stages of the disease. Elevated levels of circulating low-density lipoprotein





(legend on next page)

(LDL) cholesterol, as observed in patients with familial hypercholesterolemia (FH), are a prominent risk factor for developing atherosclerosis (Ference et al., 2017). FH is predominantly caused by loss-of-function mutations in the LDL receptor (*LDLR*) gene, leading to impaired hepatic uptake of LDL and, consequently, elevated levels of plasma LDL (Reiner, 2015). It has been shown that hypercholesterolemia affects the lipidome of macrophages and deactivates part of their inflammatory responses via activation of LXR (Spann et al., 2012). However, LXR-independent repression mechanisms still need to be defined. Here we confirm that hypercholesterolemia attenuates LPS-induced inflammatory macrophage responses and show that this deactivated phenotype is accompanied by a diminished Nrf2-mediated oxidative stress response and LXR-independent suppression of the PPP, indicating that systemic and cellular metabolism are directly intertwined, together regulating macrophage function.

## RESULTS

### Hypercholesterolemia Translates into Altered Immune Cell Metabolism

Ingenuity Pathway Analysis (IPA) of published FH patient microarray data (GEO: GSE13985; characteristics in Table S1) identified oxidative phosphorylation (OXPHOS) and mitochondrial dysfunction among the top-ranked enriched canonical pathways (Figure 1A), and most differentially expressed genes belonging to those pathways were downregulated in leukocytes of FH patients (Figure 1B).

To study the effects of systemic metabolic changes on immune cell metabolism in more detail, *Ldlr*<sup>ko</sup> mice were fed a high-fat diet (HFD) to induce hypercholesterolemia and hypertriglyceridemia or a normal-fat control diet (NFD) (Figures S1A–S1C). Peritoneal macrophages from HFD mice were elicited as a validated *in vivo* model and source of foam cells (Spann et al., 2012). CD11b<sup>+</sup>F4/80<sup>+</sup> peritoneal macrophages isolated from the HFD group were lipid-laden foam cells (hereafter referred to as “HFD macrophages”; Figures S1D and S1E) and compared with “NFD macrophages” to evaluate the effect of systemic metabolism on macrophage metabolism independent of microenvironmental cues present in atherosclerotic lesions. To study the effects of these different lipid environments on glycolysis and mitochondrial function in macrophages, we per-

formed an extracellular flux analysis and revealed similar basal glycolysis and mitochondrial respiration in macrophages isolated from mice fed either diet (Figure 1C). Interestingly, HFD macrophages demonstrated lower maximal mitochondrial respiration and a reduced spare respiratory capacity (SRC) (Figure 1D) but showed no differences in non-mitochondrial oxygen consumption, ATP production, and proton leak (Figure S2A). Furthermore, both macrophage types showed similar fuel dependencies, with fatty acids being the main drivers of mitochondrial oxygen consumption (Figure 1E).

Because reduced mitochondrial mass results in decreased SRC in T cells (van der Windt et al., 2012), we assessed whether a lower mitochondrial abundance could explain the reduced SRC in HFD macrophages. Supporting this notion, HFD macrophages indeed showed a lower mitochondrial mass, as demonstrated by MitoTracker Green staining, mitochondrial DNA:genomic DNA ratio, and mitochondrial complex immunoblotting (Figures 1F and 1G and S2B). Together with the observation that similar amounts of mitochondria isolated from NFD or HFD macrophages display equal respiration (Figure 1H), our data strongly suggest that the reduced maximal respiration in HFD macrophages is mainly due to a decrease in mitochondrial mass. RNA sequencing revealed that genes related to mitochondrial biogenesis and dynamics were not altered in HFD macrophages; this was further confirmed by qPCR and immunoblotting (Figures S2C–S2E). Pathway analysis indicated that the top most enriched pathways were related to cholesterol biosynthesis, and associated genes were downregulated in HFD macrophages (Figures 1I and 1J).

Given the importance of metabolites such as itaconate, succinate, and  $\alpha$ -ketoglutarate in regulating macrophage function (Lampropoulou et al., 2016; Liu et al., 2017; Michelucci et al., 2013; Mills et al., 2016, 2018; Tannahill et al., 2013), we next measured the levels of an extensive set of 63 metabolites. Partial least square discriminant (PLS-DA) analysis was used to discriminate NFD and HFD macrophages based on the measured metabolites. Interestingly, the abundance of several metabolites varied among NFD and HFD macrophages, with itaconate as the most distinctive metabolite (Figure 1K), whose abundance was lower in HFD macrophages (Table S2). Overall, hypercholesterolemia is associated with reduced mitochondrial mass and maximal respiration and affects the levels of metabolites such as itaconate.

### Figure 1. Hypercholesterolemia Affects Immune Cell Metabolism

- (A) Top differential IPA-annotated canonical pathways between FH patients and controls based on their differentially expressed genes (DEGs).  
 (B) Heatmap DEGs from the oxidative phosphorylation and mitochondrial dysfunction pathways.  
 (C) Basal oxygen consumption rate (OCR) and ECAR of NFD and HFD macrophages.  
 (D) Oxidative phosphorylation (OXPHOS) parameters were assessed by recording OCR after injection of oligomycin (OM), carbonyl cyanide-4-(trifluoromethoxy) phenylhydrazone (FCCP), and rotenone plus antimycin (ROT/AA). Maximal respiration and spare respiratory capacity were plotted in bar graphs (see also Figure S2A).  
 (E) Dependency of NFD and HFD macrophages to oxidize glucose (pyruvate), glutamine (glutamate), and fatty acids to fuel mitochondrial respiration, as measured by including the inhibitors UK5099, Bis-2-(5-phenylacetamido-1,3,4-thiadiazol-2-yl)ethyl sulfide (BPTES), and etomoxir, respectively.  
 (F and G) Mitochondrial mass as measured by (F) MitoTracker Green staining and (G) mtDNA:genomic DNA (gDNA) ratio (see also Figure S2B).  
 (H) Measurements of respiration of isolated mitochondria.  
 (I) Top differential IPA-annotated pathways between NFD and HFD macrophages based on DEGs.  
 (J) Heatmap of DEGs involved in cholesterol biosynthesis.  
 (K) Variable importance in projection (VIP) scores derived from PLS-DA to rank the measured metabolites on their contribution to the model. Values represent mean  $\pm$  SEM of three (C and E–H) or four mice (D). \* $p < 0.05$ , \*\* $p < 0.01$  by two-tailed Student's *t* test.



### Hypercholesterolemia Attenuates Inflammatory Macrophage Responses without Major Changes in Glycolysis or the TCA Cycle

Because itaconate regulates inflammatory macrophage responses (Jha et al., 2015; Mills et al., 2018) and was reduced in naive HFD macrophages, we investigated the effects of hypercholesterolemia on LPS-induced inflammatory macrophage activation. In parallel to the previously reported decreased expression of several inflammatory genes, we identified reduced secretion of pro-inflammatory cytokines as well as lower nitric oxide (NO) and lower ROS levels in HFD macrophages (Figures 2A–2C). Both types of macrophages exhibited similar phagocytic activity and comparable expression of *Ii10* and IL-4-induced genes and surface proteins (Figures 2D, S3A, and S3B). Together, this does not indicate a general inhibition of macrophage activation in the HFD group but shows that these cells undergo a deactivation process during which foam cells lose part of their LPS-induced inflammatory properties. Likewise, short exposure to oxidized or acetylated LDL *in vitro* also decreased subsequent LPS-induced tumor necrosis factor (TNF), IL-6, and NO secretion in NFD macrophages (Figure S3C).

To address whether distinct LPS-induced metabolic rewiring underlies the deactivated phenotype of HFD foam cells, we measured glycolysis upon acute and 24-hr LPS exposure. NFD and HFD macrophages showed comparable glycolytic rates and glucose uptake (Figure 2E, 2F, and S3D), indicating that the attenuated inflammatory phenotype of HFD macrophages is probably not caused by reduced glycolysis.

Next we examined whether differences in succinate, itaconate,  $\alpha$ -ketoglutarate, or other metabolites could explain the attenuated pro-inflammatory function of LPS-stimulated HFD macrophages. PLS-DA identified distinct metabolic profiles upon LPS stimulation in macrophages from both groups (Figure 2G). We observed that LPS induced itaconate, succinate, and oxaloacetate levels to a similar extent in both NFD and HFD macrophages (Figure 2H). This suggests that the reduced inflammatory phenotype observed in HFD macrophages is not caused by a distinct LPS-induced TCA cycle reconfiguration. In addition to altered levels of different amino acids (Figures 2I) and increased levels of NADH in HFD macrophages (Table S2), several metabolites related to the PPP (marked with asterisks in Figure 2I) strongly contributed to the differential metabolic profile in LPS-stimulated NFD and HFD macrophages.

### Hypercholesterolemia Diminishes the NRF2 and PPP in Macrophages

Metabolic analysis demonstrated an increased abundance of several PPP metabolites, including ribose-5P or ribulose-5P, sedoheptulose-7P, and glyceraldehyde 3-P upon LPS stimulation (Figure 3A). Interestingly, LPS-induced ribose-5P or ribulose-5P and sedoheptulose-7P levels were lower in HFD macrophages. Analyzing the two genes that encode glucose-6-phosphate dehydrogenase (G6PD) as the rate-limiting enzyme of the PPP in mice (Huminiecki and Wolfe, 2004) revealed that the LPS-induced elevation of *G6pd2*, but not *G6pdx*, was absent in HFD macrophages (Figures 3B and 3C). Moreover, *Pgd* (encoding 6-phosphogluconate dehydrogenase, which converts 6-phosphogluconate into ribulose 5-P in the PPP) was reduced

in both naive and LPS-stimulated HFD macrophages (Figure 3B), whereas *Pgd* protein levels were only suppressed in naive HFD macrophages (Figure S4A). To validate whether suppression of the PPP in HFD macrophages (Figure 3D) could explain their attenuated LPS-induced inflammatory responses, we pharmacologically inhibited G6PD with dehydroepiandrosterone (DHEA) or 6-aminonicotinamide (6-AN). Supporting this notion, blockade of the PPP diminished the LPS-induced production of pro-inflammatory mediators in macrophages (Figure 3E). Because desmosterol-driven LXR activation regulates at least a part of the inflammatory phenotype of foam cells (Spann et al., 2012), we studied whether this pathway controls the PPP. Activation of LXR and its target genes with GW3965 did not affect PPP genes and metabolites (Figures S4B–S4D), backing the idea that both LXR-dependent and independent mechanisms contribute to the diminished inflammatory phenotype of foam cells (Spann et al., 2012).

To uncover the LXR-independent mechanistic link between hypercholesterolemia, suppressed PPP, and inflammation, we further explored our RNA sequencing (RNA-seq) dataset. Pathways analysis revealed that the Nrf2 pathway was the most differentially regulated pathway between LPS-stimulated NFD and HFD macrophages (Figure 3F), and most genes of this pathway were downregulated in HFD macrophages (Figure 3G). Accordingly, Nrf2 protein levels were reduced in LPS-treated HFD macrophages (Figure 3H). Importantly, Nrf2 was found to be a regulator of the PPP in cancer cells (Mitsuishi et al., 2012) and analyzing expression data from Nrf2-deficient macrophages (GEO: GSE71695) revealed that several PPP genes, including *Pgd*, are downregulated in Nrf2-deficient macrophages (Figure S4E). Moreover, analysis of published chromatin immunoprecipitation (ChIP-seq) data (DDBJ: DRA003771) revealed binding of Nrf2 4 kb upstream of the *Pgd* locus (Figure 3I), suggesting a direct link between reduced Nrf2 activity and *Pgd* expression in HFD macrophages. Indeed, *Pgd* is suppressed in Nrf2-deficient macrophages and increased in macrophages that have lower levels of the Nrf2 repressor protein KEAP1 (Figure 3J). Accordingly, the LPS-induced production of sedoheptulose-7P and ribose-5P or ribulose-5P downstream of *Pgd* in the PPP was blunted in the absence of Nrf2 (Figure S4F). This suppressed Nrf2 signaling acts in parallel with other pathways, like the LXR pathway (Spann et al., 2012), and manipulating one branch does not recapitulate the deactivated phenotype observed in HFD macrophages. Indeed, Nrf2-deficient macrophages did not show overall suppressed LPS responses (Figure S4G).

Together, this demonstrates a link between reduced Nrf2 and a defective PPP in HFD macrophages and that the latter pathway supports inflammatory responses.

## DISCUSSION

Recent findings in the rapidly expanding field of immunometabolism underscored the importance of metabolic reprogramming during macrophage activation (Van den Bossche et al., 2017). However, most knowledge regarding this metabolic-immunologic crosstalk has emerged from *in vitro*-cultured macrophages, excluding different (e.g., microenvironmental and systemic) layers of regulation that are at play *in vivo*. This gave us the

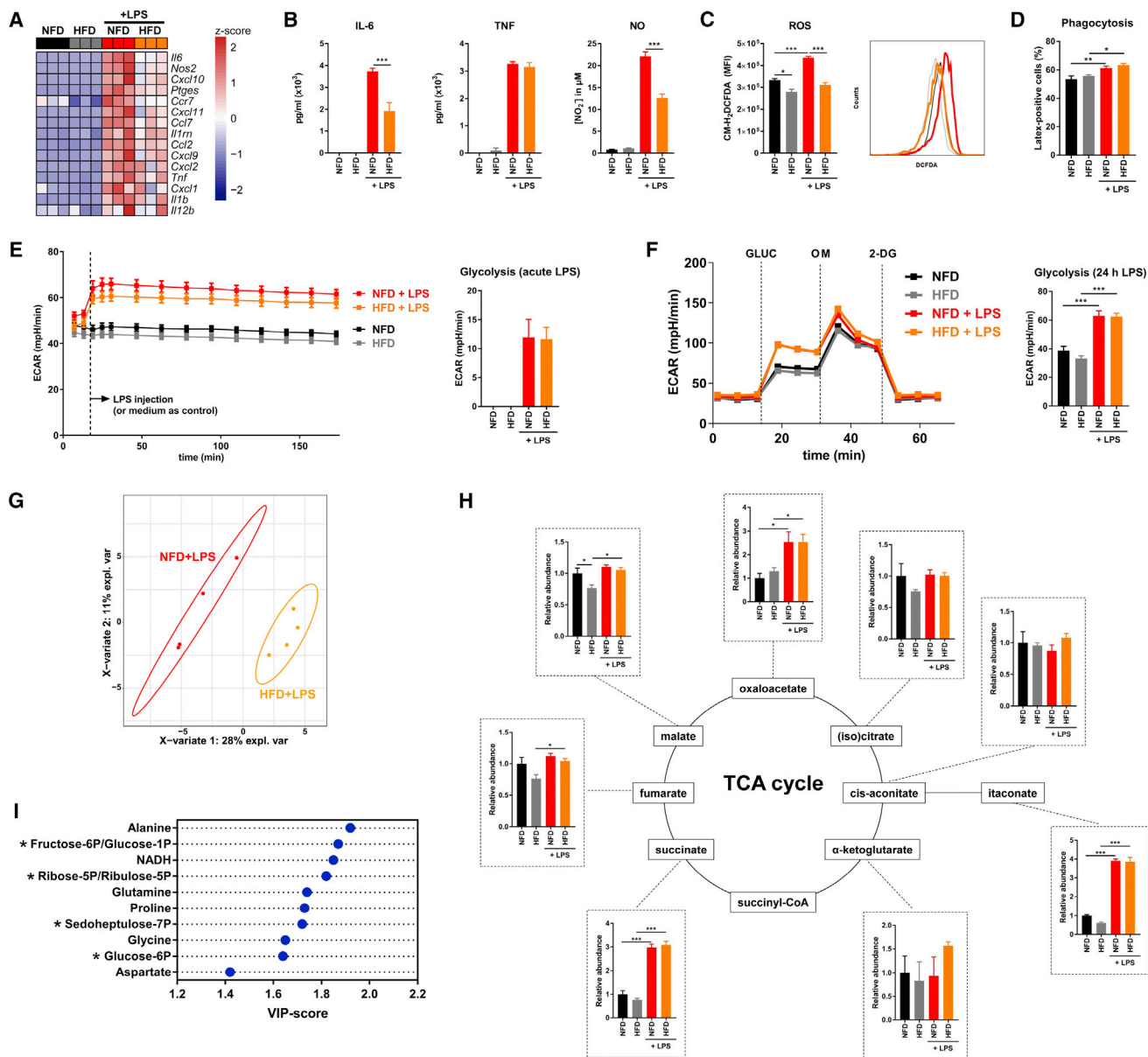


**Figure 2. Hypercholesterolemia Attenuates the Inflammatory Phenotype of Macrophages without Reconfiguring Glycolysis and the TCA Cycle**

(A) Selected inflammatory genes in LPS-stimulated NFD and HFD macrophages (IL-4 response in Figures S3A and S3B).  
 (B) Cytokine and NO production by NFD and HFD macrophages (see also Figure S3C).  
 (C) Reactive oxygen species (ROS) levels as measured with 5-(and-6)-chloromethyl-2',7'-dichlorodihydrofluorescein diacetate, acetyl ester (CM-H<sub>2</sub>DCFDA).  
 (D) Phagocytic capacity (see also Figure S3E).  
 (E) Real-time ECAR of NFD and HFD macrophages. The bar graph represents the acute LPS-induced ECAR.  
 (F) Glycolysis parameters were determined by recording the ECAR after injection of glucose, OM, and 2-deoxyglucose (2-DG). The glycolytic rate is plotted in a bar graph (glucose uptake in Figure S3D).  
 (G) PLS-DA plotted discrimination between LPS-stimulated NFD and HFD macrophages based on LC-HRMS analysis of 63 metabolites.  
 (H) Relative abundance of TCA cycle intermediates as measured by liquid chromatography-high resolution mass spectrometry (LC-HRMS).  
 (I) VIP scores derived from PLS-DA based on LPS-stimulated NFD and HFD macrophages to rank metabolites on their contribution to the model. Pentose phosphate pathway (PPP) metabolites are marked with asterisks.  
 Values represent mean  $\pm$  SEM of three (B–F) or four mice (H). One-way ANOVA; \* $p$  < 0.05, \*\* $p$  < 0.01, \*\*\* $p$  < 0.001.

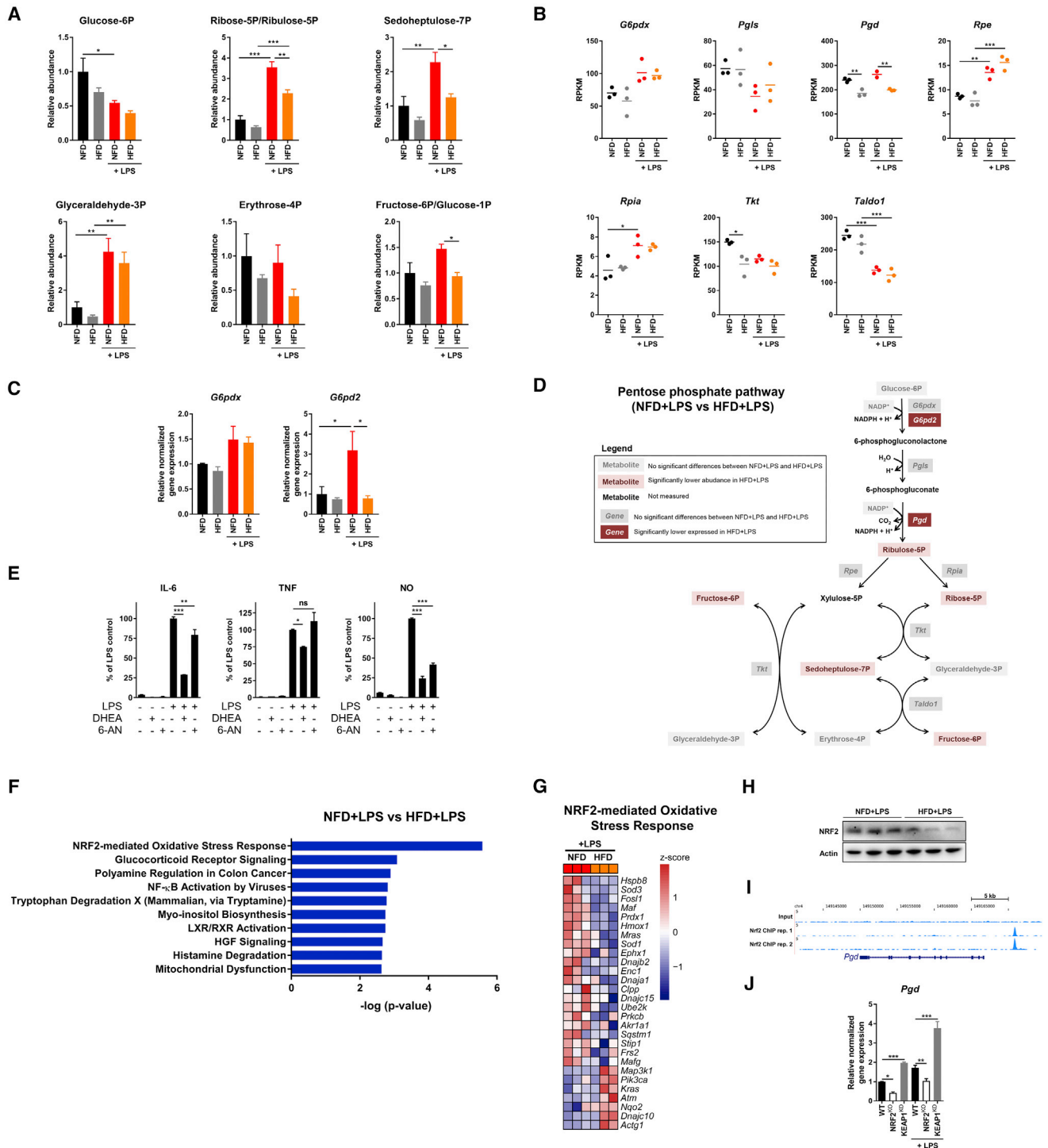


**Figure 3. Hypercholesterolemia Reduces LPS-Mediated Induction of the PPP in Macrophages**

(A) Relative abundance of PPP metabolites.  
 (B) Expression levels of genes encoding PPP enzymes represented as RPKM (reads per kilobase per million mapped reads). Horizontal lines represent mean values.  
 (C) *G6pdx* and *G6pd2* gene expression.  
 (D) Schematic representation of the abundance and expression of PPP metabolites and genes.  
 (E) Cytokine and NO production by macrophages in the absence or presence of LPS and 100  $\mu$ M G6PD inhibitor dehydroepiandrosterone (DHEA) or 6-aminonicotinamide (6-AN).

(legend continued on next page)



incentive to explore the influences of different systemic lipid environments on cellular macrophage metabolism and function.

Leukocytes from FH patients demonstrated reduced expression of genes related to OXPHOS. In mice, hypercholesterolemia was associated with reduced cholesterol biosynthesis in macrophages. Differences in cell type (total leukocytes versus macrophages) or species (human versus mouse) might underlie this discrepancy. *Dhcr24*, which encodes 24-dehydrocholesterol reductase, which converts desmosterol into cholesterol, was the most suppressed gene related to cholesterol biosynthesis in macrophages from HFD mice. This finding is in agreement with a previous study, and diminished *Dhcr24* expression was found to result in the accumulation of desmosterol in HFD macrophages (Spann et al., 2012).

Isolated macrophages from hypercholesterolemic mice showed reduced maximal respiration and SRC. In T cells, SRC is positively correlated with their survival (van der Windt et al., 2012). Therefore, decreased SRC might increase the susceptibility to apoptosis in macrophage foam cells, potentially contributing to necrotic core development in atherosclerotic lesions (Moore et al., 2013).

It is well-accepted that atherosclerosis is a chronic inflammatory disease driven by elevated LDL cholesterol levels. The Canakinumab Antiinflammatory Thrombosis Outcome Study (CANTOS) trial provides strong evidence in support of the inflammation hypothesis and demonstrated that neutralizing the pro-inflammatory cytokine IL-1 $\beta$  significantly reduces the rate of recurrent cardiovascular events (Ridker et al., 2017).

Confirming previous literature (Spann et al., 2012), we now observed that the LPS-induced secretion of inflammatory mediators was reduced in macrophages isolated from hypercholesterolemic mice. This might appear to be inconsistent with the inflammation hypothesis of atherogenesis. However, it is important to note that both *in vivo*-elicited HFD foam cells and *in vitro* LDL-exposed macrophages still produce considerable amounts of inflammatory cytokines upon activation, albeit to a lower extent than “normal” macrophages. Another explanation for the observed deactivated phenotype of foam cells could be the phenotypic diversity detected in plaques (Cochain et al., 2018). Not all plaque macrophages exhibit a pro-inflammatory phenotype, and there is a substantial subpopulation of macrophages with anti-inflammatory features (Kadl et al., 2010). In agreement with our observations, recent transcriptome analysis of macrophages from atherosclerotic aortae revealed that lipid-loaded plaque macrophages are less inflammatory than their non-foamy counterparts (Kim et al., 2018). We therefore favor the theory that, in addition to the systemic metabolic environment, microenvironmental cues regulate macrophage phenotypes in plaques (Spann et al., 2012) to promote the chronic inflammatory responses that are demonstrably driving atherogenesis.

Accumulation of cellular cholesterol leads to specific oxysterols and sterols that regulate the activity of LXR (Spann et al.,

2012). LXRs bind to and prevent the removal of repressor complexes at TLR4-responsive genes, blunting their expression and exerting anti-inflammatory effects (Ghisletti et al., 2007). We now show that, in addition to LXR (Spann et al., 2012), LXR-independent impairment of the PPP contributes to the suppressed inflammatory responses in macrophage foam cells during hypercholesterolemia.

Interestingly, we discovered that 6-phosphogluconate dehydrogenase (*Pgd*) gene expression and downstream metabolites were blunted in HFD macrophages. In accordance, knockdown of PGD was found to reduce the oxidative PPP flux, NADPH:NADP<sup>+</sup> ratio, and ribulose-5P and ribose-5P levels in human cancer cells (Lin et al., 2015). NADPH and ribose-5P generated in the PPP can support the inflammatory macrophage responses in different ways, including ROS production, anti-oxidant cellular defense, fatty acid synthesis, and nucleotide production (Nagy and Hascsemi, 2015). Thus, reduced flux through the PPP as observed in HFD macrophages can cause attenuated inflammatory responses and ROS production. Furthermore, *Pgd* expression was already reduced in naive HFD macrophages, possibly creating a condition that causes impaired future LPS responses. Vice versa, the lower PPP might also be a consequence of an attenuated inflammatory phenotype in HFD macrophages and the consecutive lower demand for PPP-derived products that regulate inflammation and anti-oxidant cellular defense.

We identified the Nrf2-mediated oxidative stress response as the most suppressed pathway in LPS-stimulated HFD macrophages. Nrf2 emerged as a crucial regulator of the inflammatory responses in macrophages (Kobayashi et al., 2016; Mills et al., 2018). Interestingly, several PPP genes were previously identified as Nrf2 target genes in cancer cells (Mitsuishi et al., 2012). Here we emphasized the importance of the Nrf2 pathway in the regulation of the PPP in macrophages. Importantly, suppressed Nrf2 is not the only mediator of the HFD macrophage phenotype and probably acts in parallel with other mechanisms, like the desmosterol-induced LXR pathway that was described earlier (Spann et al., 2012). Indeed, LXR activation or Nrf2 deletion as such did not result in the deactivated HFD macrophage phenotype. Our observations agree with previous studies demonstrating normal IL-1 $\beta$ , TNF, and IL-6 expression in the absence of Nrf2 (Mills et al., 2018; Bambouskova et al., 2018; Kobayashi et al., 2016). Conversely, activation of Nrf2 in macrophages by pharmacological or genetic (low KEAP1 expression) means clearly dampens inflammatory responses (Kobayashi et al., 2016) and mediates the anti-inflammatory effects of the metabolite itaconate (Mills et al., 2018). Thus, low levels of Nrf2 do not affect LPS responses as such, but Nrf2 activation is clearly anti-inflammatory. It will be of interest to define the mechanism responsible for Nrf2 repression in macrophage foam cells.

Together, these observations show that hypercholesterolemia suppresses the Nrf2 and PPP in macrophages and deactivates their inflammatory phenotype. We demonstrate that systemic

(F) Top differential IPA-annotated pathways between LPS-stimulated NFD and HFD based on DEGs.

(G) Heatmap of DEGs from the “NRF2-mediated oxidative stress response” IPA canonical pathway.

(H–J) NRF2 immunoblot (H), ChIP-seq binding profile of Nrf2 at the *Pgd* locus in macrophages (I), and *Pgd* expression (J) (see also Figures S4A and S4E–S4G). Values represent mean  $\pm$  SEM of three (C, E, and J) or four mice (A). One-way ANOVA; \*p < 0.05; \*\*p < 0.01; \*\*\*p < 0.001; ns, not significant.

metabolic changes translate into rewired intracellular metabolic pathways in macrophages that are tailored to support their effector functions. This highlights the intricate interplay between inflammatory signaling and metabolic pathways.

## STAR★METHODS

Detailed methods are provided in the online version of this paper and include the following:

- **KEY RESOURCES TABLE**
- **CONTACT FOR REAGENT AND RESOURCE SHARING**
- **EXPERIMENTAL MODEL AND SUBJECT DETAILS**
  - Mice
- **METHOD DETAILS**
  - Isolation of macrophages
  - Metabolic extracellular flux analysis
  - Respiratory measurements of isolated mitochondria
  - Liquid chromatography - mass spectrometry
  - Flow cytometry
  - Immunoblotting
  - Cytokine and NO production
  - RNA sequencing
  - Bioinformatics
  - qPCR
- **QUANTIFICATION AND STATISTICAL ANALYSIS**
- **DATA AND SOFTWARE AVAILABILITY**

## SUPPLEMENTAL INFORMATION

Supplemental Information includes four figures and three tables and can be found with this article online at <https://doi.org/10.1016/j.celrep.2018.10.092>.

## ACKNOWLEDGMENTS

J.V.d.B. received a VENI grant from ZonMW (91615052) and a Netherlands Heart Foundation junior postdoctoral grant (2013T003) and senior fellowship (2017T048). M.P.J.d.W. is an established investigator of the Netherlands Heart Foundation, is supported by grants from the Netherlands Heart Foundation and Spark-Holding BV (2015B002), the European Union (ITN grant EPIMAC and REPROGRAM [EU Horizon 2020]), and Fondation Leducq (16CVD-01), and holds an AMC fellowship. We acknowledge support from the Netherlands CardioVascular Research Initiative, Dutch Federation of University Medical Centers, the Netherlands Organisation for Health Research and Development, the Royal Netherlands Academy of Sciences (CVON 2011-19 and CVON 2017-20) and Cancer Research UK (C20953/A18644). We thank Tadeja Rezen, Peter Juvan, and Damjana Rozman for the GEO: GSE13985 dataset details.

## AUTHOR CONTRIBUTIONS

Conceptualization, J.V.d.B.; Methodology, J.V.d.B.; Formal Analysis, J.B., S.G.S.V., M.v.W., K.H.M.P., and J.V.d.B.; Investigation, J.B., S.v.d.V., S.G.S.V., D.G.R., R.C.I.W., A.E.N., S.W.D., M.E.W., E.V.K., and J.V.d.B.; Writing – Original Draft, J.B.; Writing – Review & Editing, J.B., S.G.S.V., D.S., R.H.H., L.A.O., A.T.D.-K., E.L., M.P.J.d.W., and J.V.d.B.; Visualization, J.B., M.v.W., and J.V.d.B.; Supervision, M.P.J.d.W. and J.V.d.B.; Funding Acquisition, M.P.J.d.W. and J.V.d.B. All authors read and approved the final manuscript.

## DECLARATION OF INTERESTS

The authors declare no competing interests.

Received: December 1, 2017  
Revised: September 11, 2018  
Accepted: October 24, 2018  
Published: November 20, 2018

## REFERENCES

- Bambouskova, M., Gorvel, L., Lampropoulou, V., Sergushichev, A., Loginicheva, E., Johnson, K., Korenfeld, D., Mathyer, M.E., Kim, H., Huang, L.H., et al. (2018). Electrophilic properties of itaconate and derivatives regulate the IkappaBzeta-ATF3 inflammatory axis. *Nature* 556, 501–504.
- Cochain, C., Vafadarnejad, E., Arampatzi, P., Jaroslav, P., Winkels, H., Ley, K., Wolf, D., Saliba, A.-E., and Zernecke, A. (2018). Single-cell RNA-seq reveals the transcriptional landscape and heterogeneity of aortic macrophages in murine atherosclerosis. *Circ. Res.* 122, 1661–1674.
- Dobin, A., Davis, C.A., Schlesinger, F., Drenkow, J., Zaleski, C., Jha, S., Batut, P., Chaisson, M., and Gingeras, T.R. (2013). STAR: ultrafast universal RNA-seq aligner. *Bioinformatics* 29, 15–21.
- Ference, B.A., Ginsberg, H.N., Graham, I., Ray, K.K., Packard, C.J., Bruckert, E., Hegele, R.A., Krauss, R.M., Raal, F.J., Schunkert, H., et al. (2017). Low-density lipoproteins cause atherosclerotic cardiovascular disease. 1. Evidence from genetic, epidemiologic, and clinical studies. A consensus statement from the European Atherosclerosis Society Consensus Panel. *Eur. Heart J.* 38, 2459–2472.
- Ghisletti, S., Huang, W., Ogawa, S., Pascual, G., Lin, M.-E., Willson, T.M., Rosenfeld, M.G., and Glass, C.K. (2007). Parallel SUMOylation-dependent pathways mediate gene- and signal-specific transrepression by LXRs and PPARgamma. *Mol. Cell* 25, 57–70.
- Heinz, S., Benner, C., Spann, N., Bertolino, E., Lin, Y.C., Laslo, P., Cheng, J.X., Murre, C., Singh, H., and Glass, C.K. (2010). Simple combinations of lineage-determining transcription factors prime cis-regulatory elements required for macrophage and B cell identities. *Mol. Cell* 38, 576–589.
- Huminiecki, L., and Wolfe, K.H. (2004). Divergence of spatial gene expression profiles following species-specific gene duplications in human and mouse. *Genome Res.* 14 (10A), 1870–1879.
- Itoh, K., Chiba, T., Takahashi, S., Ishii, T., Igarashi, K., Katoh, Y., Oyake, T., Hayashi, N., Satoh, K., Hatayama, I., et al. (1997). An Nrf2/small Maf heterodimer mediates the induction of phase II detoxifying enzyme genes through antioxidant response elements. *Biochem. Biophys. Res. Commun.* 236, 313–322.
- Jha, A.K., Huang, S.C.-C., Sergushichev, A., Lampropoulou, V., Ivanova, Y., Loginicheva, E., Chmielewski, K., Stewart, K.M., Ashall, J., Everts, B., et al. (2015). Network integration of parallel metabolic and transcriptional data reveals metabolic modules that regulate macrophage polarization. *Immunity* 42, 419–430.
- Kadl, A., Meher, A.K., Sharma, P.R., Lee, M.Y., Doran, A.C., Johnstone, S.R., Elliott, M.R., Gruber, F., Han, J., Chen, W., et al. (2010). Identification of a novel macrophage phenotype that develops in response to atherogenic phospholipids via Nrf2. *Circ. Res.* 107, 737–746.
- Kim, K., Shim, D., Lee, J.S., Zaitsev, K., Williams, J.W., Kim, K.-W., Jang, M.-Y., Jang, H.S., Yun, T.J., and Lee, S.H. (2018). Transcriptome Analysis Reveals Non-Foamy Rather than Foamy Plaque Macrophages Are Pro-Inflammatory in Atherosclerotic Murine Models. *Circ. Res.* 123, 1127–1142.
- Kobayashi, E.H., Suzuki, T., Funayama, R., Nagashima, T., Hayashi, M., Sekine, H., Tanaka, N., Moriguchi, T., Motohashi, H., Nakayama, K., and Yamamoto, M. (2016). Nrf2 suppresses macrophage inflammatory response by blocking proinflammatory cytokine transcription. *Nat. Commun.* 7, 11624.
- Lampropoulou, V., Sergushichev, A., Bambouskova, M., Nair, S., Vincent, E.E., Loginicheva, E., Cervantes-Barragan, L., Ma, X., Huang, S.C.-C., Griss, T., et al. (2016). Itaconate links inhibition of succinate dehydrogenase with macrophage metabolic remodeling and regulation of inflammation. *Cell Metab.* 24, 158–166.
- Li, H., Handsaker, B., Wysoker, A., Fennell, T., Ruan, J., Homer, N., Marth, G., Abecasis, G., and Durbin, R.; 1000 Genome Project Data Processing

- Subgroup (2009). The sequence alignment/map format and SAMtools. *Bioinformatics* 25, 2078–2079.
- Lin, R., Elf, S., Shan, C., Kang, H.-B., Ji, Q., Zhou, L., Hitosugi, T., Zhang, L., Zhang, S., Seo, J.H., et al. (2015). 6-Phosphogluconate dehydrogenase links oxidative PPP, lipogenesis and tumour growth by inhibiting LKB1-AMPK signalling. *Nat. Cell Biol.* 17, 1484–1496.
- Littlewood-Evans, A., Sarret, S., Apfel, V., Loesle, P., Dawson, J., Zhang, J., Muller, A., Tigani, B., Kneuer, R., and Patel, S. (2016). GPR91 senses extracellular succinate released from inflammatory macrophages and exacerbates rheumatoid arthritis. *J. Exp. Med.* 213, 1655–1662.
- Liu, P.-S., Wang, H., Li, X., Chao, T., Teav, T., Christen, S., Di Conza, G., Cheng, W.-C., Chou, C.-H., Vavakova, M., et al. (2017).  $\alpha$ -ketoglutarate orchestrates macrophage activation through metabolic and epigenetic reprogramming. *Nat. Immunol.* 18, 985–994.
- Love, M.I., Huber, W., and Anders, S. (2014). Moderated estimation of fold change and dispersion for RNA-seq data with DESeq2. *Genome Biol.* 15, 550.
- Michelucci, A., Cordes, T., Ghelfi, J., Pailot, A., Reiling, N., Goldmann, O., Binz, T., Wegner, A., Tallam, A., Rausell, A., et al. (2013). Immune-responsive gene 1 protein links metabolism to immunity by catalyzing itaconic acid production. *Proc. Natl. Acad. Sci. USA* 110, 7820–7825.
- Mills, E.L., Kelly, B., Logan, A., Costa, A.S., Varma, M., Bryant, C.E., Tourloumou, P., Däbritz, J.H.M., Gottlieb, E., and Latorre, I. (2016). Succinate dehydrogenase supports metabolic repurposing of mitochondria to drive inflammatory macrophages. *Cell* 167, 457–470.e13.
- Mills, E.L., Ryan, D.G., Prag, H.A., Dikovskaya, D., Menon, D., Zaslona, Z., Jedrychowski, M.P., Costa, A.S.H., Higgins, M., Hams, E., et al. (2018). Itaconate is an anti-inflammatory metabolite that activates Nrf2 via alkylation of KEAP1. *Nature* 556, 113–117.
- Mitsuishi, Y., Taguchi, K., Kawatani, Y., Shibata, T., Nukiwa, T., Aburatani, H., Yamamoto, M., and Motohashi, H. (2012). Nrf2 redirects glucose and glutamine into anabolic pathways in metabolic reprogramming. *Cancer Cell* 22, 66–79.
- Moore, K.J., Sheedy, F.J., and Fisher, E.A. (2013). Macrophages in atherosclerosis: a dynamic balance. *Nat. Rev. Immunol.* 13, 709–721.
- Nagy, C., and Haschemi, A. (2015). Time and demand are two critical dimensions of immunometabolism: the process of macrophage activation and the pentose phosphate pathway. *Front. Immunol.* 6, 164.
- Norata, G.D., Caligiuri, G., Chavakis, T., Matarese, G., Netea, M.G., Nicoletti, A., O'Neill, L.A., and Marelli-Berg, F.M. (2015). The cellular and molecular basis of translational immunometabolism. *Immunity* 43, 421–434.
- Reiner, Ž. (2015). Management of patients with familial hypercholesterolaemia. *Nat. Rev. Cardiol.* 12, 565–575.
- Ridker, P.M., Everett, B.M., Thuren, T., MacFadyen, J.G., Chang, W.H., Ballantyne, C., Fonseca, F., Nicolau, J., Koenig, W., Anker, S.D., et al.; CANTOS Trial Group (2017). Antiinflammatory Therapy with Canakinumab for Atherosclerotic Disease. *N. Engl. J. Med.* 377, 1119–1131.
- Ritchie, M.E., Phipson, B., Wu, D., Hu, Y., Law, C.W., Shi, W., and Smyth, G.K. (2015). limma powers differential expression analyses for RNA-sequencing and microarray studies. *Nucleic Acids Res.* 43, e47.
- Rogers, G.W., Brand, M.D., Petrosyan, S., Ashok, D., Elorza, A.A., Ferrick, D.A., and Murphy, A.N. (2011). High throughput microplate respiratory measurements using minimal quantities of isolated mitochondria. *PLoS ONE* 6, e21746.
- Rohart, F., Gautier, B., Singh, A., and Lê Cao, K.-A. (2017). mixOmics: An R package for 'omics feature selection and multiple data integration. *PLoS Comput. Biol.* 13, e1005752.
- Spann, N.J., Garmire, L.X., McDonald, J.G., Myers, D.S., Milne, S.B., Shibata, N., Reichart, D., Fox, J.N., Shaked, I., Heudobler, D., et al. (2012). Regulated accumulation of desmosterol integrates macrophage lipid metabolism and inflammatory responses. *Cell* 151, 138–152.
- Taguchi, K., Maher, J.M., Suzuki, T., Kawatani, Y., Motohashi, H., and Yamamoto, M. (2010). Genetic analysis of cytoprotective functions supported by graded expression of Keap1. *Mol. Cell. Biol.* 30, 3016–3026.
- Tannahill, G.M., Curtis, A.M., Adamik, J., Palsson-McDermott, E.M., McGettrick, A.F., Goel, G., Frezza, C., Bernard, N.J., Kelly, B., Foley, N.H., et al. (2013). Succinate is an inflammatory signal that induces IL-1 $\beta$  through HIF-1 $\alpha$ . *Nature* 496, 238–242.
- Thévenot, E.A., Roux, A., Xu, Y., Ezan, E., and Junot, C. (2015). Analysis of the human adult urinary metabolome variations with age, body mass index, and gender by implementing a comprehensive workflow for univariate and OPLS statistical analyses. *J. Proteome Res.* 14, 3322–3335.
- Van den Bossche, J., Baardman, J., and de Winther, M.P. (2015). Metabolic characterization of polarized M1 and M2 bone marrow-derived macrophages using real-time extracellular flux analysis. Published online November 28, 2015. 10.3791/53424.other
- Van den Bossche, J., Baardman, J., Otto, N.A., van der Velden, S., Neele, A.E., van den Berg, S.M., Luque-Martin, R., Chen, H.-J., Boshuizen, M.C., Ahmed, M., et al. (2016). Mitochondrial dysfunction prevents repolarization of inflammatory macrophages. *Cell Rep.* 17, 684–696.
- Van den Bossche, J., O'Neill, L.A., and Menon, D. (2017). Macrophage immunometabolism: where are we (going)? *Trends Immunol.* 38, 395–406.
- van der Windt, G.J., Everts, B., Chang, C.-H., Curtis, J.D., Freitas, T.C., Amiel, E., Pearce, E.J., and Pearce, E.L. (2012). Mitochondrial respiratory capacity is a critical regulator of CD8 $^{+}$  T cell memory development. *Immunity* 36, 68–78.
- Wickham, H. (2016). ggplot2: Elegant Graphics for Data Analysis (Springer).
- Wu, F., Tymi, K., and Wilson, J.X. (2008). iNOS expression requires NADPH oxidase-dependent redox signaling in microvascular endothelial cells. *J. Cell. Physiol.* 217, 207–214.
- Wüst, R.C., de Vries, H.J., Wintjes, L.T., Rodenburg, R.J., Niessen, H.W., and Stienen, G.J. (2016). Mitochondrial complex I dysfunction and altered NAD(P)H kinetics in rat myocardium in cardiac right ventricular hypertrophy and failure. *Cardiovasc. Res.* 111, 362–372.

## STAR★METHODS

### KEY RESOURCES TABLE

REAGENT or RESOURCE	SOURCE	IDENTIFIER
<b>Antibodies</b>		
anti-actin	Millipore	Cat# MAB1501; RRID:AB_2223041
anti-mitofusin 1 (MFN1)	Abcam	Cat# ab57602; RRID:AB_2142624
anti-mitofusin 2 (MFN2)	Sigma	Cat# WH0009927M3; RRID:AB_1842440
anti-OPA1	BD Biosciences	Cat# 612606; RRID:AB_612606
anti-NRF2	Cell Signaling	Cat# 12721; RRID:AB_2715528
anti-PGD	Abcam	Cat# ab129199; RRID:AB_11144133
Total OXPHOS Rodent WB Antibody Cocktail	Abcam	Cat# ab110413; RRID:AB_2629281
anti-rabbit IgG/HRP (secondary)	Thermo Fisher Scientific	Cat# 32260; RRID:AB_1965959
anti-mouse IgG/HRP (secondary)	Thermo Fisher Scientific	Cat# 32230; RRID:AB_1965958
anti-mouse CD71-PE	BD PharMingen	Cat# 553267; RRID:AB_394744
anti-mouse CD206-APC	Biolegend	Cat# 141707; RRID:AB_10896057
anti-mouse CD273-PE	BD PharMingen	Cat# 557796; RRID:AB_396874
anti-mouse CD301-Alexa Fluor-647	Serotec	Cat# MCA2392A647T; RRID:AB_1101873
rat IgG2a-PE (isotype control)	BioLegend	Cat# 400507
rat IgG2a-APC (isotype control)	BioLegend	Cat# 400511
anti-mouse CD11b-PE-Cy7	BD PharMingen	Cat# 552850; RRID:AB_394491
anti-mouse F4/80-APC-eFluor780	eBioscience	Cat# 47-4801; RRID:AB_2637188
anti-mouse CD16/CD32 (Fc-block)	eBioscience	Cat# 14-0161; RRID:AB_467132
<b>Chemicals, Peptides, and Recombinant Proteins</b>		
Penicillin-Streptomycin	Thermo Fisher Scientific	Cat# 15140-122
L-glutamine	Thermo Fisher Scientific	Cat# 25030024
Recombinant murine IL-4	PeproTech	Cat# 214-14
Lipopolysaccharides (LPS)	Sigma	Cat# L2637
Oil Red O	Sigma	Cat# O0625
Hematoxylin	Merck	Cat# 1.05175.2500
Oligomycin (OM)	Sigma	Cat# 75351
2-deoxyglucose (2-DG)	Sigma	Cat# D6134
Carbonyl cyanide 4-(trifluoromethoxy)phenylhydrazone (FCCP)	Sigma	Cat# C2920
Rotenone	Sigma	Cat# R8875
Antimycin A	Sigma	Cat# A8674
Pyruvic acid	Sigma	Cat# 107360
Malic acid	Sigma	Cat# M0875
Adenosine diphosphate (ADP)	Sigma	Cat# A5285
MitoTracker Green FM	Thermo Fisher Scientific	Cat# M7514
CM-H <sub>2</sub> DCFDA	Thermo Fisher Scientific	Cat# C6827
2-(N-(7-Nitrobenz-2-oxa-1,3-diazol-4-yl)Amino)-2-Deoxyglucose (2-NBDG)	Thermo Fisher Scientific	Cat# N13195
RNA-free DNase	QIAGEN	Cat# 79254
6-Aminonicotinamide (6-AN)	Sigma	Cat# A68203
Dehydroepiandrosterone (DHEA)	Sigma	Cat# D063
GW3965	Sigma	Cat# G6295
<b>Critical Commercial Assays</b>		
IL-6 ELISA	Life Technologies	Cat# CMC0063
TNF ELISA	Life Technologies	Cat# CMC3013

(Continued on next page)

**Continued**

REAGENT or RESOURCE	SOURCE	IDENTIFIER
Griess reaction	Sigma	Cat# G4410
BCA Protein Assay kit	Thermo Fisher Scientific	Cat# 23225
RNeasy Mini Kit	QIAGEN	Cat# 74106
Ovation Mouse RNA-Seq System	NuGEN	Cat# 0348-32
High Pure RNA Isolation Kit	Roche	Cat# 11828665001
iScript cDNA Synthesis Kit	Bio-Rad	Cat# 170-8891
Quick-gDNA MiniPrep	Zymo Research	Cat# D3024
Deposited Data		
RNA-sequencing data	This paper	GEO: GSE107412
Experimental Models: Organisms/Strains		
Mouse: Ldlr <sup>KO</sup> ; B6.129S7-Ldlr <sup>tm1Her</sup> /J	The Jackson Laboratory	JAX:002207
Mouse: Nr1h2 <sup>KO</sup> ; B6.129P3-Nr1h2 <sup>tm1Mym</sup>	<a href="#">Itoh et al., 1997</a>	N/A
Mouse: Keap1 <sup>KD</sup> ; B6.129P3-Keap1 <sup>tm2Mym</sup>	<a href="#">Taguchi et al., 2010</a>	N/A
Mouse: WT: C57BL/6J	The Jackson Laboratory	JAX:000664
Oligonucleotides		
Primer sequences	This paper ( <a href="#">Table S3</a> )	N/A
Software and Algorithms		
FlowJo	ThreeStar	N/A
GraphPad Prism 7	GraphPad Software	N/A
Seahorse Wave	Agilent	N/A
Ingenuity Pathway Analysis	QIAGEN	N/A
R package: ggplot2	<a href="#">Wickham, 2016</a>	<a href="https://cran.r-project.org/web/packages/ggplot2">https://cran.r-project.org/web/packages/ggplot2</a>
R package: ropis	<a href="#">Thévenot et al. (2015)</a>	<a href="http://www.bioconductor.org/packages/release/bioc/html/ropis.html">http://www.bioconductor.org/packages/release/bioc/html/ropis.html</a>
R package: mixOmics	<a href="#">Rohart et al. (2017)</a>	<a href="http://mixomics.org">http://mixomics.org</a>
STAR 2.5.2b	<a href="#">Dobin et al. (2013)</a>	<a href="https://github.com/alexdobin/STAR/releases">https://github.com/alexdobin/STAR/releases</a>
SAM tools	<a href="#">Li et al. (2009)</a>	<a href="http://samtools.sourceforge.net">http://samtools.sourceforge.net</a>
HOMER	<a href="#">Heinz et al. (2010)</a>	<a href="http://homer.ucsd.edu/homer">http://homer.ucsd.edu/homer</a>
R package: DESeq2	<a href="#">Love et al. (2014)</a>	<a href="https://bioconductor.org/packages/release/bioc/html/DESeq2.html">https://bioconductor.org/packages/release/bioc/html/DESeq2.html</a>
R package: limma	<a href="#">Ritchie et al. (2015)</a>	<a href="https://bioconductor.org/packages/release/bioc/html/limma.html">https://bioconductor.org/packages/release/bioc/html/limma.html</a>
Other		
Control normal fat diet (NFD)	Harlan Laboratories (Envigo)	Cat# 2016 (Teklad global 16% protein)
High fat diet (HFD)	Special diet Services	Code 824199
0.5 μM Fluoresbrite YG microspheres	Polysciences	Cat# 17152
Thioglycollate medium	Fisher Scientific	Cat# 11782834
RPMI-1640 medium	Thermo Fisher Scientific	Cat# 52400041
RPMI-1640 Medium, no glucose	Thermo Fisher Scientific	Cat# 11879020
Fetal Bovine Serum	Thermo Fisher Scientific	Cat# 10500
NP-40 cell lysis buffer	Thermo Fisher Scientific	Cat# FNN0021
Protease Inhibitor Cocktail	Sigma	Cat# 11873580001
PhosSTOP	Sigma	Cat# 4906837001
Bolt 4-12% Bis-Tris Plus Gels	Thermo Fisher Scientific	Cat# NW04120BOX
Nitrocellulose Membrane	Bio-Rad	Cat# 162-0094
TWEEN 20	Sigma	Cat# P1379
SuperSignal West Pico PLUS Chemiluminescent Substrate	Thermo Fisher Scientific	Cat# 34580
Fast SYBR Green Master Mix	Applied Biosystems	Cat# 4385618



## CONTACT FOR REAGENT AND RESOURCE SHARING

Further information and requests for resources and reagents should be directed to and will be fulfilled by the Lead Contact, Jan Van den Bossche ([j.vandenbossche@vumc.nl](mailto:j.vandenbossche@vumc.nl)).

## EXPERIMENTAL MODEL AND SUBJECT DETAILS

### Mice

Female and male *Ldlr*<sup>KO</sup> mice were obtained from Jackson Laboratory. *Ldlr*<sup>KO</sup> mice were housed at the Animal Research Institute AMC (ARIA) and all animal experiments were conducted after approval (permit: DBC102861) by the Committee for Animal Welfare of the Academic Medical Center, University of Amsterdam. 6-month old adult mice were used for experiments and put on a control normal fat diet (NFD, 4% fat, Harlan Laboratories) or a high fat, high cholesterol diet (HFD, 16% fat, 0.25% cholesterol, Special Diet Services) for 10 weeks. *Nrf2*-knockout (*Nrf2*<sup>KO</sup>) ([Itoh et al., 1997](#)) and *Keap1*-knockdown (*Keap1*<sup>KD</sup>) ([Taguchi et al., 2010](#)) mice, and their wild-type (WT) counterparts, all 8-12-week old females on the C57BL/6 genetic background, were bred and maintained in the Medical School Resource Unit of the University of Dundee. Mice of the same sex were randomly assigned to both experimental groups in disposable Innovive 101 IVC cages in groups of 3 or 4.

## METHOD DETAILS

### Isolation of macrophages

After 10 weeks of NFD or HFD, *Ldlr*<sup>KO</sup> mice were euthanized by CO<sub>2</sub> asphyxiation. Four days prior to sacrifice, mice were intraperitoneally injected with 3% thioglycollate medium (Fisher Scientific). Upon sacrifice, the peritoneum was flushed with 10 mL ice-cold PBS and collected peritoneal cells were cultured in RPMI-1640 containing 25 mM HEPES, 2 mM L-glutamine, 10% FCS, 100 U/ml penicillin and 100 µg/ml streptomycin (GIBCO). After 3 h, non-adherent cells were washed away and adhered cells (typically consisting of 90%–95% CD11b<sup>+</sup> F4/80<sup>+</sup> macrophages, [Figure S1D](#)) were stimulated for 24 hours with 10 ng/ml LPS (Sigma) or 100 U/ml IL-4 (Peprotech), or were left untreated, and were used for further analyses. Blood cholesterol and triglyceride levels were measured by enzymatic methods using available kits (Roche). To determine lipid accumulated in peritoneal macrophages, tissue slides with cells were fixed in 4% formalin for 10 minutes and washed two times with PBS (with magnesium and chloride) before and after fixation. Subsequently, tissue slides were incubated in 60% isopropanol for 15 minutes before staining for 45 minutes with fresh 0.3% Oil Red O in 60% isopropanol. After staining, tissue slides were rinsed in 60% isopropanol, washed in distilled water, incubated for 1 minute with hematoxylin blue in tap water and rinsed with distilled water. Bone-marrow derived (BMDM) macrophages were generated from femurs and tibia from WT, *Nrf2*<sup>KO</sup> and *Keap1*<sup>KD</sup> mice and differentiated in RPMI-1640 containing 25 mM HEPES, 2 mM L-glutamine, 10% FCS, 100 U/ml penicillin and 100 µg/ml streptomycin and 15% L929-conditioned medium for 7 days.

### Metabolic extracellular flux analysis

Macrophages (1 × 10<sup>5</sup> cells/well) were plated on XF-96-cell culture plates (Seahorse Bioscience) and treated as specified. OCR and ECAR were assessed using the XF-96 Flux Analyzer (Seahorse Bioscience) as detailed before ([Van den Bossche et al., 2015](#)). Changes in ECAR in response to glucose (10 mM), OM (1.5 µM) and 2-DG (100 mM) injection were used to calculate all glycolysis parameters and OXPHOS characteristics were calculated from the OCR changes in response to OM (1.5 µM), FCCP (1.5 µM) and rotenone (1.25 µM) + antimycin A (2.5 µM) injection ([Van den Bossche et al., 2015](#); [Van den Bossche et al., 2016](#)). The Seahorse Bioscience Mito Fuel Flex Test Kit was used to determine the dependency of cells for glucose, glutamine or fatty acid oxidation.

### Respiratory measurements of isolated mitochondria

To isolate mitochondria, cell pellets were resuspended in 1 mL of MTE buffer (250 mM mannitol, 5 mM TRIS, 0.5 mM EDTA, pH 7.4). Macrophages were lysed using 10 passages through the cell cracker (European Molecular Biology Laboratory, Heidelberg, Germany). The homogenate was centrifuged 10 min at 1000 g, after which the supernatant was transferred to a new tube and centrifuged at 10000 g. The resulting supernatant was considered the cytosolic fraction. The final pellet containing the mitochondrial fraction was washed with 1 mL MTE buffer, centrifuged at 3600 g and resuspended in a minimal volume of MTE buffer. Equal amounts of mitochondria (0.5 µg/well) were resuspended in MAS buffer (70 mM sucrose, 220 mM mannitol, 10 mM KH<sub>2</sub>PO<sub>4</sub>, 5 mM MgCl<sub>2</sub>, 2 mM HEPES, and 1 mM EGTA; pH 7.2, plus 10 mM pyruvate and 1 mM malate as substrates), transferred to XF-96-cell culture plates, centrifuged at 2000 g for 20 min at 4°C and measured using a XF-96 Flux Analyzer (Seahorse Bioscience) to assess basal oxygen consumption (state 2), maximal coupled respiration or state 3 after injection of 4 mM ADP, state 4o after injection of 1.5 µM OM, maximal uncoupled respiration (state 3u) after injection of 4 µM FCCP and the respiratory control ratio (RCR = state 3/state 4o) in accordance to an established protocol ([Rogers et al., 2011](#)).

### Liquid chromatography - mass spectrometry

Macrophages (5 × 10<sup>5</sup> cells/well) in 24 well plates were washed three times with 0.9% NaCl. Metabolism was quenched by adding 1 mL ice-cold methanol/water (1/1; v/v). The following internal standards were added, D<sub>3</sub>-aspartic acid, D<sub>3</sub>-serine, D<sub>5</sub>-glutamine,

D<sub>3</sub>-glutamate, <sup>13</sup>C<sub>3</sub>-pyruvate, <sup>13</sup>C<sub>6</sub>-isoleucine, <sup>13</sup>C<sub>6</sub>-glucose, <sup>13</sup>C<sub>6</sub>-fructose-1,6-biphosphate, <sup>13</sup>C<sub>6</sub>-glucose-6-phosphate, adenosine-<sup>15</sup>N<sub>5</sub>-monophosphate and guanosine-<sup>15</sup>N<sub>5</sub>-monophosphate (5 μM). 1 mL of chloroform was added, vortexed and centrifuged for 5 minutes at 14,000 rpm at 4°C. ~800 μL of the “polar” top layer was transferred to a 1.5 mL tube, dried to dryness in a vacuum concentrator and dissolved in 100 μL methanol/water (6/4; v/v). For the analysis, we used a Thermo Scientific (U)HPLC system coupled to a Thermo Q Exactive (Plus) Orbitrap mass spectrometer (Waltman) with a SeQuant ZIC-cHILIC column at 15°C (PEEK 100 × 2.1 mm, 3.0 μm particle size, Merck). The mobile phase composed of (A) 9/1 acetonitrile/water with 5 mM ammonium acetate; pH 6.8 and (B) 1/9 acetonitrile/water with 5 mM ammonium acetate; pH 6.8, respectively. The LC program started with 100% (A) hold 0–3 min; ramping 3–24 min to 20% (A); hold from 24–27 min at 20% (A); ramping from 27–28 min to 100% (A); and re-equilibrate from 28–35 min with 100% (A), flow rate was 0.250 mL/min. The MS data were acquired in full scan, negative ionization mode with a mass resolution of 140,000. Interpretation of the data was performed in the Xcalibur software (ThermoFisher). Subsequent analyses were done in a R environment using the *ggplot2*, *ropls* and *mixOmics* packages (Rohart et al., 2017; Thévenot et al., 2015; Wickham, 2016).

### Flow cytometry

To assess surface marker expression, cells (1.5 × 10<sup>5</sup> cells/well) in 96 well plates were detached with citrate and transferred to V-bottom 96 well plates and stained with CD71, CD206, CD273, CD301 or isotype controls (all 1:250 diluted in PBS with 0.5% BSA and 2.5 mM EDTA) for 20 minutes at room temperature in the dark. After labeling, cells were washed with PBS with 0.5% BSA and 2.5 mM EDTA and finally resuspend in PBS with 0.5% BSA and 2.5 mM EDTA and measured on BD FACSCanto or a Beckman Coulter CytoFLEX, and analyzed using FlowJo (TreeStar). In order to quantify mitochondrial mass and ROS production, macrophages (10<sup>5</sup> cells/well) in 96 well plates were detached using citrate buffer (17 mM tri-Sodium citrate dehydrate and 135 mM potassium chloride in water) transferred to V-bottom 96 well plates and washed with PBS. Next, cells were resuspended in PBS with 200 nm MitoTracker Green or 20 μM CM-H<sub>2</sub>DCFDA (both ThermoFisher) and incubated for 30 minutes at 37°C (5% CO<sub>2</sub>). After incubation, cells were washed with PBS and mitochondrial mass and ROS production was measured using flow cytometry. To determine glucose uptake, macrophages (10<sup>5</sup> cells/well) were cultured in 96 well plates for two hours in RPMI-1640 lacking glucose and serum. Subsequently, 2-NBDG (ThermoFisher) was added for an additional incubation of 20 minutes in a final concentration of 25 μM. Next, cells were detached with citrate buffer, transferred to V-bottom 96 well plates and washed with PBS and analyzed using flow cytometry. To assess phagocytic activity, 10<sup>5</sup> macrophages were cultured for 1 h at 37°C (or 4°C as a control, Figure S3E) in the presence of Fluoresbrite YG microspheres (0.5 μM, Polysciences).

### Immunoblotting

Immunoblotting for NRF2 and mitochondrial complexes was performed as detailed by (Mills et al., 2018) and (Wüst et al., 2016), respectively. For MFN1, MFN2, OPA1 and PGD immunoblotting, macrophages (1 × 10<sup>6</sup> cells/well) in 12 well plates were lysed in NP40 cell lysis buffer (ThermoFisher) supplemented with protease inhibitor cocktail (Sigma-Aldrich) and PhosSTOP (Sigma-Aldrich). Lysates were equalized on protein concentration after quantification with the BCA assay (ThermoFisher), separated on Bolt 4%–12% Bis-Tris gels (ThermoFisher) and transferred onto nitrocellulose membranes (Bio-Rad). After blocking for 1 hour with 5% milk powder (Campina) in Tris-buffered saline, TWEEN 20 (TBS-T), membranes were incubated overnight with primary antibodies against MFN1 (1:1000 dilution), MFN2 (1:200), OPA1 (1:1000) and PGD (1:1000) in 5% milk, TBS-T, followed by incubation for 1 hour with horseradish peroxidase (HRP)-conjugated secondary antibodies (1:2000) in 5% milk, TBS-T and visualization with SuperSignal West Pico Chemiluminescent PLUS Substrate (Thermo Fisher Scientific).

### Cytokine and NO production

IL-6 and TNF levels in the supernatant were measured by ELISA (Life Technologies) and NO production was assessed by a Griess reaction (Sigma-Aldrich) according to the supplier's protocol.

### RNA sequencing

Total RNA was isolated from peritoneal macrophages using a RNeasy Mini Kit with DNase treatment (QIAGEN). Strand-specific libraries were constructed from 100 ng total RNA using ‘Ovation RNA-Seq system’ following manufacturer instructions (NuGen Technologies). Samples were pooled and diluted to 10 nM and sequenced on an Illumina HiSeq 4000 instrument (Illumina) to a depth of ± 20 million single-ended 50 bp reads.

### Bioinformatics

Reads were aligned to the mouse genome mm10 by STAR 2.5.2b with default settings (Dobin et al., 2013). BAM files were indexed and filtered on MAPQ > 15 with SAMTools 1.3.1 (Li et al., 2009). Raw tag counts and RPKM (reads per kilobase per million mapped reads) values per gene were summed using HOMER2's analyzeRepeats.pl script with default settings and the -oadj or -rpkm options for raw counts and RPKM reporting, respectively (Heinz et al., 2010). Differential expression was assessed using the DESeq2 bioconductor package in an R 3.3.1 environment with gene expression called differential with a *p* value < 0.05 and an average RPKM > 1 in at least one group (Love et al., 2014). Presented RPKM values in scatterplots were tested using one-way ANOVA followed by Bonferroni's post hoc comparisons test. Differential expression analysis on available microarray data (GEO: GSE13985)

was executed using the *limma* package and gene expression was called differential with a p value < 0.05 (Ritchie et al., 2015). Differential expressed genes were analyzed in Ingenuity Pathway Analysis (Qiaqen) to identify deregulated pathways.

### qPCR

RNA was isolated with High Pure RNA Isolation kits (Roche), cDNA was synthesized with iScript (Bio-Rad), and qPCR was performed using SYBR Green Fast mix (Applied Biosystems) on a ViiA7 (Applied Biosystems). Housekeeping genes *Rplp0* and *Ppia* were used for normalization and used primer sequences are noted in the Table S3. DNA was extracted using the Quick-gDNA MiniPrep (Zymo Research) kit and primers for *mt-Co1* and *Ndufv1* were used to determine the mtDNA/gDNA ratio.

### QUANTIFICATION AND STATISTICAL ANALYSIS

All data are presented as mean  $\pm$  standard error of the mean (SEM). Number (n) and type (biological or technical) of replicates are indicated in the figure legends. Data were tested using a two-tailed Student's t test (when comparing two groups) or one-way ANOVA followed by Bonferroni's post hoc comparison to test multiple groups in GraphPad Prism version 7.0 software, as indicated in the figure legends. p values < 0.05 were considered significant, with levels of significance being indicated as follows: \*p < 0.05; \*\*p < 0.01; \*\*\*p < 0.001; ns, not significant.

### DATA AND SOFTWARE AVAILABILITY

The accession number for the RNA sequencing data reported in this paper is GEO: GSE107412.